Micromagnetic simulations of magnetostatically coupled Nickel nanowires

Riccardo Hertel[a)]
Max-Planck-Institute of Microstructure Physics, Weinberg 2, 06120 Halle, Germany

(Received 24 May 2001; accepted for publication 17 August 2001)

Magnetic structures and magnetization processes in arrays of closely packed Ni nanowires (length $l=1$ μm, diameter $d=40$ nm, and period: 100 nm) are investigated by means of micromagnetic modelling. The simulations are performed with an algorithm based on the finite element method combined with the boundary element method which allows for the accurate calculation of magnetostatic interactions. Magnetization states of Ni nanowires at zero field are calculated. Only few, simple magnetization configurations result to be stable. Transient states of the magnetization indicate that magnetization reversal occurs by means of nucleation at the ends of the particles and subsequent soliton propagation. Hysteresis loops of up to 16 interacting nanowires are simulated. It turns out that magnetostatic interactions between the wires have a significant influence on the switching field. © *2001 American Institute of Physics.* [DOI: 10.1063/1.1412275]

I. INTRODUCTION

Recently developed techniques for fabricating regular arrays of magnetic wires have given rise to several studies on the interesting magnetic properties of these systems.[1–4] Not much is known about the details of the magnetization processes occurring in arrays of closely packed magnetic nanowires. Even in single nanowires, surprisingly involved domain structures can be found.[4] The problem becomes highly complex when the long-range magnetostatic coupling between the wires is considered.[2,3] Therefore, modeling of such systems is often subject to strong simplifications. For instance, the magnetostatic interaction is sometimes treated by assuming that the wires may be regarded as dipoles.[2] In other cases, the magnetization reversal mode of magnetic wires is assumed to be a uniform rotation.[5] Though many of the models based on simplifying assumptions yield good agreement with experimental observation, their physical validity is not clear.

On the other hand, rigorous micromagnetic simulations have been performed for single, isolated nanowires and elongated particles.[6–8] In these cases, the magnetostatic interaction of neighboring wires was generally omitted from the simulation.

In this article a different approach is presented to study the magnetic structure and the hysteretic properties of Nickel nanowires. Instead of attempting to mimic an infinitely extended array of wires using more or less plausible simplifications, a magnetostatically coupled ensemble consisting of a comparatively small number of wires is modeled without making simplifying assumptions concerning the magnetic structure or the dipolar fields. It is understood that the restriction to a limited number of nanowires makes it difficult to relate the results directly to an infinitely extended array. This procedure, however, allows one to analyze in detail the effect of magnetostatic interactions from first principles by placing an increasing number of wires on lattice sites and investigating the influence of the number of interacting wires on the hysteretic properties like, e.g., the switching field of the array.

The material and the geometry chosen for the simulations is inspired by experimental studies performed recently by Nielsch *et al.*[9] According to these experiments, the following model has been chosen for the simulation:

(i) A regular, hexagonal array of wires is assumed. The center-to-center spacing between the wires is 100 nm.

(ii) The diameter of the wires is 40 nm, their length is 1 μm.

(iii) The wires consist of nearly amorphous Nickel. Hence, magnetocrystalline anisotropy is neglected. An exchange constant $A=1.05\times10^{-11}$ J/m and a saturation polarization $J_s=|\boldsymbol{J}|=0.52$ T have been chosen to simulate the micromagnetic properties of Ni.

A possible technical application of ordered arrays of magnetic nanowires is a perpendicular data storage medium. This is probably better realized with shorter wires. If the magnetization state of a nanowire is used as an information unit, the writing process could become problematic if the wires are too long. In order to compare the computed results to the experiments, however, the geometry of the wires has been chosen as just described above.

II. MICROMAGNETIC BACKGROUND AND NUMERICAL METHOD

Equilibrium structures of the magnetization are characterized by local energy minima. The total energy E_{tot} of a given arrangement of the magnetization in a ferromagnetic sample reads

$$E_{\mathrm{tot}}=E_{\mathrm{an}}+E_{\mathrm{exc}}+E_{\mathrm{dem}}+E_{\mathrm{Zee}} \quad , \tag{1}$$

where the terms on the right-hand side denote the anisotropy energy, the exchange energy, the stray field energy, and the Zeeman energy, respectively. These contributions are usually sufficient for micromagnetic simulations. For given material

a)Electronic mail: hertel@mpi-halle.mpg.de

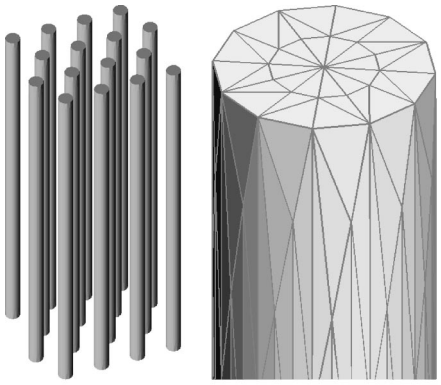

FIG. 1. (a) An array of nanowires as used in the calculation. (b) Magnified view on the top of one wire. The lines represent the edges of the finite elements.

parameters and the external field $\boldsymbol{H}_{\text{ext}}$, the total energy (1) of a ferromagnetic sample is uniquely determined by the directional field of the polarization $\boldsymbol{J}$ within the sample. Since the anisotropy in the case considered here is set to zero, the total energy of the sample writes[10]

$$E_{\text{tot}}=\int_{(V)}\sum_{i=x,y,z} A\cdot(\nabla \boldsymbol{m}_i)^2-\frac{1}{2}\boldsymbol{H}_{\text{d}}\cdot\boldsymbol{J}-\boldsymbol{H}_{\text{ext}}\cdot\boldsymbol{J}\,\text{d}V. \qquad (2)$$

Here V, is the volume of the sample and $\boldsymbol{m}_i$ are the Cartesian components of the reduced magnetization $\boldsymbol{m}=\boldsymbol{J}/|\boldsymbol{J}|$. The vector field $\boldsymbol{H}_{\text{d}}$ denotes the stray field which is discussed next.

The principle of the algorithm consists in minimizing the total energy by varying the direction of the polarization $\boldsymbol{J}$ at discrete points and thus obtaining an approximation of an equilibrium arrangement of the magnetization.

A. Discretization

For the calculation, a discretized form of Eq. (2) is used. The volume integration becomes a sum of integrals over subregions, i.e., the finite elements. The polarization $\boldsymbol{J}$, discretized at the nodes of the finite element mesh, is interpolated linearly within each element. Tetrahedral elements of irregular shape are used.

Each nanowire is subdivided into 10 020 finite elements. Figure 1(a) shows an array of nanowires as it is used in the simulation. The discretization mesh is shown in Fig. 1(b). The circular cross section can be approximated very well using relatively few discretization points. This is an example for the geometrical flexibility of the finite element method. Regular cube-shaped discretization cells which are typically used in finite difference methods would require a much higher number of cells in order to approximate the shape realistically.

The triangulation is performed using QHULL.[11] Some effort has to be made to remove and correct degenerate elements which result from the triangulation if the body is not strictly convex. After this first triangulation, the mesh is further refined using a longest-edge bisection scheme.[12] To build up a regular array of nanowires, the same mesh is used for each nanowire which is "replicated" by shifting the position of the nodes.

B. Energy minimization

The minimization of the total energy (2) has to be performed with the constraint of constant magnitude of the polarization $|\boldsymbol{J}|=J_{\text{s}}=\text{const}$. This is achieved by representing the local polarization vector with polar angles

$$\boldsymbol{J}^{(i)}=J_{\text{s}}\times\begin{pmatrix}\sin\vartheta_i\cos\varphi_i\\ \sin\vartheta_i\sin\varphi_i\\ \cos\vartheta_i\end{pmatrix}, \qquad (3)$$

and minimizing the total energy with respect to ϑ and φ at each node i.

The numerical implementation of the exchange energy term is of the type

$$E_{\text{exc}}=\sum_{k=x,y,z}\boldsymbol{j}_k\cdot X\cdot\boldsymbol{j}_k, \qquad (4)$$

where the components of the vectors $\boldsymbol{j}_x$, $\boldsymbol{j}_y$, and $\boldsymbol{j}_z$ are the Cartesian x, y, and z components, respectively, of $\boldsymbol{J}^{(i)}(\vartheta_i,\varphi_i)/J_s$ at each node i according to Eq. (3), i.e., the discretized directional field of the magnetization. The matrix X is sparse which allows a fast evaluation of this energy term at low memory requirements even for large problems.

The discretized form of the Zeeman term is

$$E_{\text{Zee}}=-\sum_{i=1,N}\boldsymbol{H}_{\text{ext}}\cdot\boldsymbol{J}(\vartheta_i,\varphi_i)\cdot\Delta V_i, \qquad (5)$$

where the summation is extended over all nodes and ΔV_i is the volume assigned to each node i.

Both, the exchange energy and Zeeman term can be minimized easily by means of the conjugate gradient method which needs to be supplied by the gradients $\partial E/\partial\vartheta_i$ and $\partial E/\partial\varphi_i$.[13]

The same holds, in principle, for the stray field energy. However, the stray field $\boldsymbol{H}_{\text{d}}$ is a nonlocal function of the magnetic structure, so that this energy term becomes too complex for a direct evaluation, let alone the determination of the gradients. Therefore, the stray field is determined separately by means of a magnetic scalar potential, as discussed in the next section. For a given magnetic structure the stray field $\boldsymbol{H}_{\text{d}}$ is calculated. After this, the magnetic structure is relaxed to an energetic minimum assuming a stationary demagnetizing field. The stray field is updated after the magnetization has relaxed. In practice, the energy minimization is interrupted after a maximum of 50 iterations and a refreshment of the stray field is performed in order to maintain a close correlation between the magnetic structure and the stray field. The process is repeated until convergence is reached, i.e., till the minimization routine is not able to further reduce the total energy. The termination criterion for the minimization is a fractional tolerance parameter which signals that the minimization is completed if the routine fails to

decrease the function value by more than this amount on one iteration. Numerical experiments have shown that a relative tolerance of 10^{-8} is suitable.

C. Calculation of the demagnetizing field

The stray field is derived from a scalar potential U according to

$$\boldsymbol{H}_{\mathrm{d}} = -\boldsymbol{\nabla} U. \tag{6}$$

The scalar potential for a given magnetic configuration is obtained by solving Poisson's equation

$$\Delta U = \frac{1}{\mu_0} \boldsymbol{\nabla} \cdot \boldsymbol{J}. \tag{7}$$

The boundary conditions

$$U_{\mathrm{i}}|_{\partial V} = U_{\mathrm{o}}|_{\partial V}, \tag{8}$$

$$\left.\frac{\partial U_{\mathrm{i}}}{\partial \hat{\boldsymbol{n}}}\right|_{\partial V} - \left.\frac{\partial U_{\mathrm{o}}}{\partial \hat{\boldsymbol{n}}}\right|_{\partial V} = \frac{1}{\mu_0} \hat{\boldsymbol{n}} \cdot \boldsymbol{J}, \tag{9}$$

and

$$\lim_{x \to \infty} U = 0 \tag{10}$$

need to be considered, where U_{i} and U_{o} are the inward and the outward limit of the potential at the surface ∂V and $\hat{\boldsymbol{n}}$ is the normal vector directed out of the sample.

The problem (7)–(10) is treated by splitting the potential into a sum of two potentials $U = U_1 + U_2$. Poisson's Eq. (7) is solved for U_1 with Neumann boundary conditions (9), setting $U_1 = 0$ outside the magnetic particle. The values of U_2 at the surface can be obtained from the result of U_1 by means of a boundary integral. With these Dirichlet boundary conditions, Laplace's equation is solved for U_2.

Fredkin and Koehler were the first who applied this method to micromagnetic problems. They have provided a detailed description on this finite element method combined with the boundary element method to calculate magnetostatic fields.[14] Besides the high accuracy, this method has the advantage of allowing one to calculate the magnetostatic interaction of separate particles without the need to discretize the nonmagnetic area in between.[15] This feature is very profitable for the calculation of magnetostatically coupled magnetic wires as presented here.

Numerically, the elliptic differential equations are solved using the Galerkin method which yields a sparse symmetric system of linear equations that can be solved numerically, e.g., with the biconjugate gradient method.[13] All matrices involved in the calculation are sparse except for one dense matrix B which is used to calculate the potential at the boundary,

$$\boldsymbol{\Phi_2} = B \boldsymbol{\Phi_1}. \tag{11}$$

The vectors Φ_1 and Φ_2 contain the values of the potential U_1 and U_2 at the boundary nodes, respectively. This matrix has the rank $N_s \times N_s$ (N_s: number of nodes at the surface) and can become of considerable size. Storage of this matrix may even exceed the available memory of the computer. This is not a problem since at no time during the calculation is the *complete* matrix required. In the present calculation, the matrix is written and read in bundles of 500 rows and the matrix multiplication (11) is split up accordingly. Care must be taken to calculate the matrix elements of B with high precision. As pointed out by Fredkin and Koehler,[14] this can be achieved either by means of numerical integration or by using analytic formulas.[16] After trying both methods, the latter has been chosen because for growing rank of B, the time required for the preprocessing grows tremendously in the case of numerical integration if a reasonable order of interpolation (about 16) is used. The matrix B—like all other matrices used in the program—needs to be calculated only once during the preprocessing.

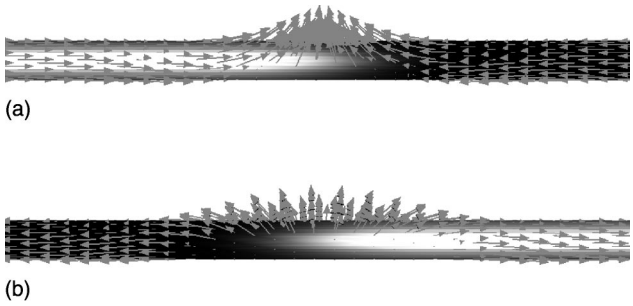

FIG. 2. Head-on domain walls resulting from the simulation. (a) Magnetization of the domains oriented towards the wall and (b) away from the wall.

III. SINGLE, ISOLATED NI WIRE

A. Zero field states

To investigate the possible stable magnetic structures in a single nanowire, the energy minimization is performed at zero external field starting with completely random initial configurations. This procedure has been successful in finding possible magnetic structures in thin film elements and ferromagnetic cubes.[17]

The special geometry of the sample does not allow for significantly diverse magnetic structures. The dominant effect of the demagnetizing field (''shape anisotropy'') favors an alignment of the magnetic moments parallel to the symmetry axis. Hence, if the magnetic structure of the wire is subdivided in magnetic domains, the domains are regions with magnetization in the direction of the symmetry axis. Except for minor deviations at the ends of the wires, the only inhomogeneous structures which result from the simulation are head-on domain walls as shown in Fig. 2, the junctions between the domains are 180° walls. This type of domain wall is a typical soliton, which propagates without changing shape when exposed to an external magnetic field. An azimuthal torsion of the magnetic structure within the domain wall is not observed. The domain wall structure does not differ for the case that the magnetization in the adjacent domains is directed towards or away from the domain wall, only the direction of the magnetization is opposed. A combination of two 180° wall types is shown in Fig. 3. The resulting 360° wall is possibly one type of magnetic structure which leads to periodic contrasts as observed experimentally by magnetic force microscopy.[4]

FIG. 3. A 360° wall may also be found as a metastable magnetization distribution.

Nucleation, propagation, and orientation of solitons is crucial for the magnetization reversal process, as will be discussed in Sec. III C.

B. Hysteresis

Hysteresis loops are investigated by applying external fields ranging from $+500$ to -500 mT and back to $+500$ mT in different directions. The field is reduced (incremented) in steps of ± 5 mT after a converged state is found. This is a quasistatic simulation, i.e., dynamic effects of the magnetization reversal are not considered. Due to the special geometry, the term shape anisotropy in this case is reasonable, and the direction along the wire may be regarded as an easy axis of the magnetization. Therefore, in the following, the hysteresis loops are labeled as ''easy axis'' and ''hard axis'' loops according to the case when the field is applied nominally parallel or perpendicular to the wire axis, respectively. Figure 4 shows a hysteresis loop of nearly perfect rectangular shape where the field is applied nominally parallel to the wire axis.

To avoid artificial, highly symmetric magnetic structures, the direction of the external field is slightly tilted off the z axis (2°) in the case of the easy axis loops. This procedure has become common in numerical micromagnetic simulations.[18]

For the easy axis loop, a remarkably high coercive field of $\mu_0 H_{\text{ext}} \simeq 142$ mT results. The coercivity is solely due to shape anisotropy, since magnetically the wire is assumed to be ideally soft. The hysteresis has a pronounced rectangular shape. This indicates that the wire switches between two homogeneously magnetized states.

In the hard axis case, the remanent state of a nanowire is not unique. Two different zero field states have been found after the wire was technically saturated perpendicular to its axis by an external field of 500 mT. The wire may either drop in a two-domain state with a 180° wall in the middle (Fig. 2) or in a single-domain state with homogeneous magnetization parallel to its axis. Since the hard axis loops do not give significant insight in the physical processes, they are omitted here. In both cases of hard axis hysteresis loops (single domain and two-domain remanent state), the wire saturates technically at a field strength of about 260 mT.

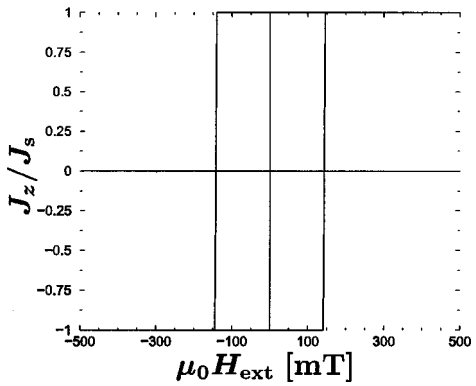

FIG. 4. A hysteresis loop of nearly perfect rectangular shape is obtained in the case of a single wire. The field is applied nominally parallel to the wire axis (easy axis loop).

C. Magnetization reversal

If an external field of sufficient strength is applied parallel to the wire, the magnetization reverses in a characterisic way. Nucleation starts at the ends of the wires. When the nucleation field is reached, the magnetization at the very end of the wire rotates out of the axis and finally reverses. While this happens, the rest of the sample remains mostly homogeneously magnetized antiparallel to the field. The reversal at one end of the sample leads to the formation of a soliton which then propagates through the wire, thus reversing the complete magnetic structure. The code used for the calculation does not account for dynamic effects. A dynamic algorithm is desirable in order to determine the switching time. Moreover, precessional effects during the soliton propagation could reveal interesting features. These topics will be addressed in future investigations. Nevertheless, the nucleation mechanism can be observed also by analyzing the transient states of the magnetization during the energy minimization as the routine modifies the magnetization towards the energetic minimum. Recent studies[19] show that the reversal mechanism by means of nucleation and propagation is also found when Gilbert's equation of motion for the magnetic moments is integrated numerically.

Six transient states of the magnetization reversal of a single Ni wire are shown in Fig. 5. From the left- to right-hand side of Figs. 5, the wires represent nonequilibrium magnetization states obtained with an increasing number of iterations. The color scaling indicates the local component of the magnetization in the direction of the wire axis. In this case, two solitons are created, one at each end. This process is inverse to a soliton–antisoliton nucleation.[20] More frequently, the formation of a single soliton is observed. The switching of Nickel nanowires with this diameter is clearly not given by the classical reversal modes curling and uniform rotation. With increasing wire diameter, the onset of a curling reversal mode is expected.

IV. HEXAGONAL ARRAY OF WIRES

By placing an increasing number of nanowires on hexagonal lattice sites the effect of magnetostatic coupling on the hysteresis loops is studied.

A. Easy axis loops

For the easy axis loops, the following tendencies result for an increasing number of nanowires: (i) The coercive field decreases, (ii) the remanence decreases, and (iii) the saturation field increases. In other words, the rectangular hysteresis loop of a single nanowire becomes narrower and sheared when the magnetostatic interaction of the wires is taken into account.

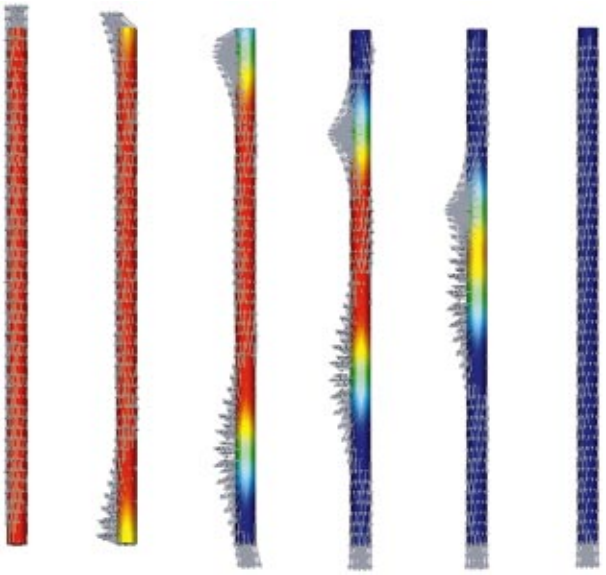

FIG. 5. (Color) Magnetization reversal of a single Ni wire. The external field is $\mu_0 H_{ext} = 145\,\mathrm{mT}$. The magnetization is reversed by means of a nucleation–propagation process.

The coercivity ranges from $\mu_0 H = 142.5\,\mathrm{mT}$ for a single nanowire to $\mu_0 H = 115.0\,\mathrm{mT}$ for the case of 16 nanowires, which is the largest set used in the calculation (cf. Fig. 6). The aivailable data is not sufficient to convincingly extrapolate a value of the coercive field for the case $N \to \infty$ (N: Number of interacting nanowires). The experimental result[9] for the coercive field of a large array of magnetic nanowires with the parameters as assumed here is $\mu_0 H_C = 100\,\mathrm{mT}$. In the simulation, this value is approached well with an increasing number of interacting wires, whereas a single nanowire results in having a significantly higher coercive field.

The normalized remanence of arrays of a different size is shown in Fig. 7. Clearly, the remanence is reduced with an increasing number of interacting wires as a consequence of magnetostatic interaction. The effect, however, is very small, which is attributed to the small number of nanowires.

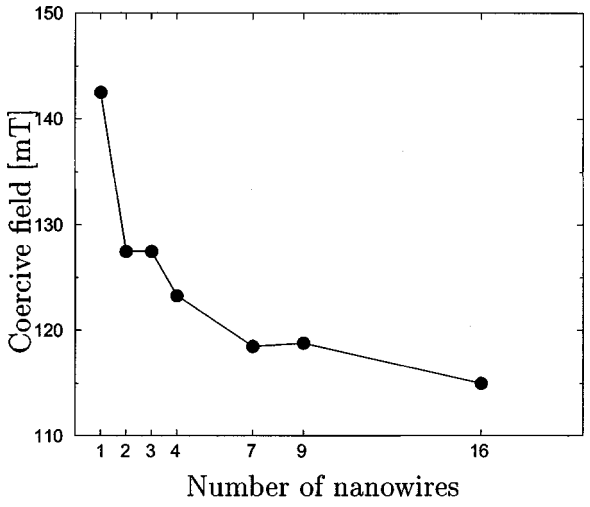

FIG. 6. The coercive field decreases with an increasing number of interacting wires.

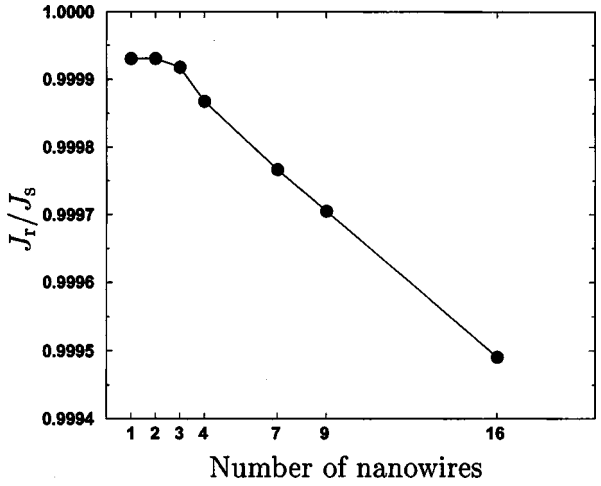

FIG. 7. Slow but continuous reduction of the remanence with an increasing number of interacting wires.

The last of the aforementioned effects of magnetostatic coupling on the easy axis hysteresis loop, i.e., the increase of the saturation field, is less evident from the obtained data. An increase from 130 mT for two interacting wires to 150 mT for nine interacting wires is observed. Calculations on significantly larger arrays are currently not feasible due to the numerical costs. It is helpful to look at the magnetic structure of a ''large'' set consisting of 16 wires near the coercive field to elucidate this effect. Figure 8 shows the magnetization state of 16 nanowires after saturation and subsequent application of a reversed field $\mu_0 H_{ext} = 120\,\mathrm{mT}$. Half of the wires have switched in direction of the applied field. Note that this field is not strong enough to switch a single decoupled wire, cf. Fig. 4. The reversal of some wires occurs because the stray field of neighboring wires adds to the external field and leads to a higher field to which the magnetic moments are effectively exposed as compared to a single nanowire. For the same reason, the magnetic structure of an ensemble as shown in Fig. 8 is more stable with respect to an external field than a single wire. If a magnetic field is applied in the direction of the axis of symmetry which is strong enough to switch most of the wires, those wires which are still magnetized antiparallel to the field are confronted with the stray field of the reversed wires which is oriented opposite to the external field and hence reduces the local field.[21] Therefore, saturation is reached at higher field strength compared to a single wire.

B. Hard axis loops

Magnetostatic coupling affects the shape of the hard axis loops qualitatively in the same way as just described for the case of the easy axis loops. However, since the hard axis hysteresis loops are already narrow and show only very small values for coercivity and remanence, the shape of the hysteresis loops hardly changes with the number of wires. A typical hard axis hysteresis loop is shown in Fig. 9.

FIG. 8. (Color) Perspective view on 16 nanowires near the coercive field. The colors represent the z component of the magnetization: The blue wires have switched while the red wires are magnetized in their original state. The small yellow regions indicate the onset of magnetization reversal.

The remanent state of the wires is usually a two-domain state with a 180° wall in the middle. These domain states result from magnetostatic coupling between the wires. If an ensemble of wires is technically saturated perpendicular to the wire axis by means of a sufficiently strong external field H_{ext}, the stray field of this arrangement is inhomogeneous at the ends of the wires. As the external field is reduced to zero, these inhomogeneities align the magnetization in opposite

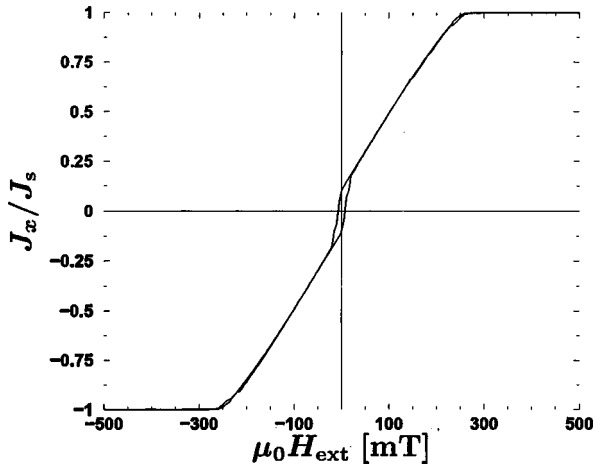

FIG. 9. Hysteresis loop of a coupled set of seven nanowires. The field is applied perpendicular to the symmetry axis.

FIG. 10. (Color) Zero field magnetization state of an array of nine nanowires after saturation perpendicular to the wire axis. The magnetic configuration of the wires is split in two domains.

directions within each wire, leading—in general—to a two-domain state, cf. Fig. 10. The origin of magnetic domains with an opposite orientation is similar to the formation of radial magnetization components in a ''flower state'' in a cube-shaped ferromagnetic sample,[22] where a homogeneous magnetization leads to an inhomogeneous demagnetizing field near the edges. In fact, a similar inhomogeneous arrangement of the magnetization has been reported previously for isolated, elongated permalloy particles near saturation in the hard axis direction.[23] These simulations also yielded inhomogeneous magnetic structures at zero field after a field of sufficient strength was applied in the hard axis direction, and corresponding experiments[24] have confirmed this behavior. Due to magnetostatic coupling, however, in a set of closely packed wires, the inhomogeneity spreads over the whole array and the symmetry of the magnetic structure within each single wire of the array is broken. This leads to a distribution of wires which, after switching off the hard axis field, drop into different magnetization states, namely of the type (a) and (b) in Fig. 2.

Hysteresis is determined mainly by the reversal of domain walls in the middle of the wire. A magnetization rever-

sal in unison is not observed for the complete set. In some cases, however, not all of the wires of an array split into domains.

V. CONCLUSIONS

Using a micromagnetic algorithm based on the finite element combined with the boundary element method, hysteresis loops, and magnetization states of magnetostatically coupled Nickel nanowires can be simulated without making use of simplifying assumptions. The most pronounced influence of magnetostatic coupling on the shape of the hysteresis loops of an ensemble of wires is the reduction of the coercive field with an increasing number of interacting wires. Only if the magnetostatic interaction of several wires is considered, the coercive field of the array approaches the experimental value well. Head-on domain walls and 360° walls can be found at zero external field, depending on the initial conditions of the calculation. These 360° domain walls could be the origin of periodic magnetic structures observed in single nanowires which are reported in the literature. The reversal mechanism in the easy axis case is given by a nucleation–propagation process which starts at the ends of the wires. Once a set of wires has been saturated parallel to the axis, inhomogeneous states of single wires only occur as transient states, and in equilibrium states all wires are homogeneuosly magnetized (though not necessarily in the same direction). According to these results, it appears to be acceptable to treat the magnetostatic interaction with a model of interacting dipoles, a procedure which is frequently used in the literature in the absence of a better model. The apparent validity of this assumption is remarkable since the wires used in this simulation are comparatively long (1 μm). Contrary to this, the results show that due to spontaneous domain formation, such a model may not be useful after the set is saturated perpendicular to the wire axis.

ACKNOWLEDGMENTS

Valuable discussions with K. Nielsch, R. Wehrspohn, and J. Kirschner are acknowledged.

[1] R. Skomski, H. Zeng, M. Zheng, and D. J. Sellmyer, Phys. Rev. B **62**, 3900 (2000).
[2] J. Velázquez, C. García, M. Vázquez, and A. Hernando, J. Appl. Phys. **85**, 2768 (1999).
[3] L. Sampaio, E. H. C. P. Sinnecker, G. R. C. Cernicchiaro, M. Knobel, M. Vázquez, and J. Velázquez, Phys. Rev. B **61**, 8976 (2000).
[4] L. Belliard, J. Miltat, A. Thiaville, S. Dubois, J. Duvail, and L. Piraux, J. Magn. Magn. Mater. **190**, 1 (1998).
[5] Y. Jaccard, P. Guitienne, D. Kelly, J.-E. Wegrowe, and J.-P. Ansermet, Phys. Rev. B **62**, 1141 (2000).
[6] C. Seberino and H. Bertram, J. Appl. Phys. **85**, 5543 (1999).
[7] R. Ferré, K. Ounadjela, J. George, L. Piraux, and S. Dubois, Phys. Rev. B **56**, 14066 (1997).
[8] D. Hinzke and U. Nowak, J. Magn. Magn. Mater. **221**, 365 (2000).
[9] K. Nielsch, R. B. Wehrspohn, J. Barthel, J. Kirschner, U. Gösele, S. F. Fischer, and H. Kronmüller, Appl. Phys. Lett. **79**, 1360 (2001).
[10] W. F. Brown, Jr., *Micromagnetics* (Wiley, New York, 1963).
[11] C. B. Barber and H. Huhdanpaa, QHULL, *Version 2.6*, available at http://www.geom.umn.edu/software/qhull, The Geometry Center (University of Minnesota) and Harvard University, 1999.
[12] R. Hertel and H. Kronmüller, IEEE Trans. Magn. **34**, 3922 (1998).
[13] W. H. Press, B. P. Flannery, S. A. Teukolsky, and W. T. Vetterling, *Numerical Recipies: The Art of Scientific Computing* (Cambrige University Press, New York, 1986).
[14] D. R. Fredkin and T. R. Koehler, IEEE Trans. Magn. **26**, 415 (1990).
[15] D. Süß, T. Schrefl, J. Fidler, and J. Chapman, J. Magn. Magn. Mater. **196**, 617 (1999).
[16] D. A. Lindholm, IEEE Trans. Magn. **20**, 2025 (1984).
[17] R. Hertel, Ph.D. thesis, University of Stuttgart, 1999.
[18] R. D. McMichael and M. J. Donahue, *Standard problem number 1, Problem specification and reported solutions*, Micromagnetic Modeling Activity Group, http://www.ctcms.nist.gov/~rdm/mumag.html, 1997.
[19] R. Hertel (unpublished).
[20] H. -B. Braun, J. Appl. Phys. **85**, 6172 (1999).
[21] Y. Ishii and M. Sato, J. Magn. Magn. Mater. **82**, 309 (1989).
[22] M. E. Schabes and H. N. Bertram, J. Appl. Phys. **64**, 1347 (1988).
[23] D. R. Fredkin, T. R. Koehler, J. F. Smyth, and S. Schultz, J. Appl. Phys. **69**, 5276 (1991).
[24] J. Smyth, S. Schultz, D. Fredkin, D. Kern, S. Rishton, H. Schmid, M. Cali, and T. Koehler, J. Appl. Phys. **69**, 5262 (1991).